INCREASED ADHESION OF CML CELLS BY ABL1 TYROSINE KINASE INHIBITORS INDUCE TUNNELING NANOTUBES

Maria Omsland[1], Vibeke Andresen[1], Maria del Pilar Ayuda Duran[2], Stein-Erik Gullaksen[1], Randi Hovland[3], Jorrit Enserink[2] and Bjørn Tore Gjertsen[1,4]*

[1]Centre for Cancer Biomarkers (CCBIO), Department of Clinical Science, University of Bergen, Bergen, Norway, [2] Department of Molecular Cell Biology, Institute for Cancer Research, The Norwegian Radium Hospital, Oslo University Hospital, Montebello, Oslo, Norway, [3]Department of Medical Genetics, Haukeland University Hospital, Bergen, Norway [4]Department of Internal Medicine, Haukeland University Hospital, Bergen, Norway.

*Corresponding author: Centre for Cancer Biomarkers, Department of Clinical Science, University of Bergen, N-5021 Bergen, Norway Email: bjorn.gjertsen@uib.no, tel: +47-55975000, fax: +47-55972950.

Running title: TKIs induce TNTs in CML cells

Keywords: (5) Chronic myeloid leukemia (CML), Tunneling nanotubes (TNTs), Tyrosine kinase inhibitors (TKIs), Interleukins, Cell adhesion.

Abstract

The actin-containing cell-to-cell communicator tunneling nanotube (TNT) is suggested to be involved in regulation of cell death threshold of leukemic cells, while the mechanism of TNT regulation is mostly unknown. We have investigated TNT formation and its response to treatment with the tyrosine kinase inhibitors (imatinib and nilotinib) in chronic myeloid leukemia (CML) cells with the pathognomonic chimeric fusion kinase BCR-ABL1. Bone marrow cells of chronic phase CML patients and CML cell lines (Kcl-22 and K562) formed few or no TNTs. Imatinib treatment induced TNT formation in both cell lines and the induction of TNTs was found to be related to increased adherence to fibronectin coated surfaces by restoration of β1-integrin function. Co-culturing of Kcl-22 cells with stromal cells or conditioned medium inhibited the TKI-induced TNT formation. Interleukin-8 (CXCL8) secreted by the stromal cells was responsible for the TNT-inhibitory effect. This suggests modulation of TNT cell-cell communication in CML tumor-host interactions as a novel mechanism in kinase inhibitor therapy of CML.

Introduction

Chronic myeloid leukemia (CML) is a myeloid stem cell disease characterized by the BCR-ABL1 fusion protein derived from the chromosomal translocation t(9;22), involving bone marrow and spleen in the chronic phase. The role of BCR-ABL1 in impaired communication between cells in the microenvironment (Bhatia, McGlave et al., 1995, Gordon, Dowding et al., 1987) is less understood in the context of the efficient therapies with small molecule kinase inhibitors that emerged at the millennium (Hochhaus, Larson et al., 2017).

The BCR-ABL1 protein has a filamentous (F)-actin binding domain and orchestrates several cellular processes involving actin processing, cell attachment to fibronectin and cell migration (Wertheim, Perera et al., 2003). Features of CML progenitor cells from patients in the chronic phase include increased motility and low affinity to fibronectin coated surfaces compared to normal counterparts (Verfaillie, McCarthy et al., 1992). Interferon alpha (IFNα), previously pivotal in CML therapy, increase adhesion of CML progenitor cells to bone marrow stromal cells (Dowding, Guo et al., 1991). Attenuated cellular mobility seems therefore to be a significant mechanism of action in effective CML therapy, recently revisited in the effective therapeutic combination of a tyrosine kinase inhibitor (TKI) and IFNα eradicating CML progenitor cells resulting in non-detectable disease (Hjorth-Hansen, Stentoft et al., 2016, Simonsson, Gedde-Dahl et al., 2011).

It is well established that the tumor microenvironment plays a pivotal role in the outcome of cancer therapy (Joyce & Pollard, 2009). While the effect of hormones and growth factors on tumor survival is relatively well characterized, the effect of physical interactions is much less understood. One such form of physical interaction is the tunneling nanotube (TNT) (Rustom, Saffrich et al., 2004). TNTs are defined as thin (50-200 nm), fragile and dynamic structures,

consisting of plasma membrane and F-actin. They are involved in cell-cell interaction and intercellular transport of organelles and viral particles (Gurke, Barroso et al., 2008, Rustom et al., 2004, Sowinski, Jolly et al., 2008). Leukocytes, their leukemic counterparts and bone marrow stromal cells have all been reported to form TNTs *in vitro* (Andresen, Wang et al., 2013, Chauveau, Aucher et al., 2010, Matula, Nemeth et al., 2016, Omsland, Bruserud et al., 2017, Onfelt, Nedvetzki et al., 2004, Polak, de Rooij et al., 2015, Reichert, Scheinpflug et al., 2016). TNTs facilitate transport of mitochondria between healthy cells and suggested to have an anti-apoptotic function (Ahmad, Mukherjee et al., 2014, Wang & Gerdes, 2015). TNTs might represent a mechanism for chemo resistance in e.g. by transport of oncoproteins as shown between T and B cells (Rainy, Chetrit et al., 2013) or by transfer of mitochondria from endothelial cells to chemotherapy exposed cancer cells (Pasquier, Guerrouahen et al., 2013). The impact of TNTs *in vivo* is so far not well characterized, but it has been described to connect myeloid cells in the cornea of mouse (Chinnery, Pearlman et al., 2008, Seyed-Razavi, Hickey et al., 2013) and in resected solid tumors from patients with malignant pleural mesothelioma and lung adenocarcinoma *in vivo* (Lou, Fujisawa et al., 2012).

Here, we characterized the function of BCR-ABL1 formation on TNTs in CML cells. We found low TNT numbers in CML cells, while treatment with the ABL1 inhibitor imatinib swiftly induced TNT formation. Mechanism of TNT formation involved increased fibronectin dependent adhesion through β1-integrin and reduced CXCL8 signaling, proposing a role for a BCR-ABL1 modulation of actin in TNT regulation that may provide a novel mechanism for effective CML therapy.

Results

TNT formation in Kcl-22 cells is significantly increased following treatment with IFNα or TKIs

In order to investigate the presence of TNTs between CML cells, primary bone marrow CML cells were cultured for 24 h on fibronectin coated surfaces and TNTs were quantified as earlier described for acute myeloid leukemia (AML) cells (Omsland et al., 2017). When we compared number of TNTs/100 cells in bone marrow cells derived from four different patients diagnosed with CML (P1-P4), very few TNTs were detected and the cells appeared mobile and morphologically spherical (Fig 1A and Supplemental Fig 1A).

Treatment of CML cells with IFNα or TKIs have been reported to increase cell adherence to fibronectin (Dowding et al., 1991, Obr, Roselova et al., 2014). Cell adherence has also been suggested to correlate with TNT formation (Reichert et al., 2016). Based on this, we examined the CML cell lines Kcl-22 and K562, before and after treatment for 24 h with pre-apoptotic doses of IFNα or the ABL1 specific TKIs imatinib or nilotinib (Druker, Tamura et al., 1996, Weisberg, Manley et al., 2005). To enable live imaging of TNTs the cell lines were stably transduced to express a cellular membrane localized GFP (memGFP). The untreated K562 cells showed highest TNT formation capabilities with 3.8 TNTs/100 cells compared to only 0.8 TNTs/100 cells for the untreated Kcl-22 cells (Fig 1B). The untreated K562 cells also seemed to adhere more strongly to the fibronectin-coated surfaces compared to Kcl-22 cells appearing morphologically spherical (Supplemental Fig S1B). Following IFNα treatment (100 U/ml) for 24 h, the Kcl-22 cells changed morphology, with increased adherence and cellular stretching in addition the number of TNTs increased from 0.8 TNTs/100 cells to 6.8 TNTs/100 cells. Interestingly, similar results

were not observed for the K562 cells (Fig 1B). Time-lapse microscopy after 1 h treatment with IFNα demonstrated GFP positive dots moving along the TNTs, from one cell to another, indicating that these TNTs could function as transport devices (Fig 1C and Supplementary video 1). Next, we treated Kcl-22 and K562 cells for 24 h with pre-apoptotic concentrations of imatinib (5 µM) or nilotinib (100 nM) and quantified the number of TNTs compared to untreated cells. Imatinib treatment induced TNT formation in both cell lines, while nilotinib treatment induced TNT formation in Kcl-22 cells only (Fig 1D). Cell viability after TKI treatment was verified by Hoechst staining, the K562 was the most sensitive cell line towards nilotinib treatment for 24 h (16.9 % for K562 and 10.2 % for Kcl-22) and we therefore investigated 1 hour treatment with nilotinib (100 nM) however, TNT induction was only observed in the Kcl-22 cells (Fig 1E).

Scanning electron microscopy revealed that the TNTs were thin cell-to-cell connecting structures which could contain bulges, indicating potential intercellular transport (Fig 1F, arrow). Immunofluorescence microscopy of nilotinib-treated Kcl-22 cells (1 h) revealed the presence of F-actin and the absence of β-tubulin in the TNTs (Fig 1G). The nilotinib-treated Kcl-22 cells also went through a change in morphology from spherical semi-attached cells to more spread-out and firmly attached cells (Fig 1G). The critical role of F-actin in these TNTs was further examined by treating the cells with the actin polymerization inhibitor cytochalasin D (CytD (Casella, Flanagan et al., 1981)). Kcl-22 cells were treated for 24 h with nilotinib (100 nM) and quantified for TNTs before treatment with CytD (2µM) for 20 min followed by a second TNT quantification (Fig 1H). This demonstrated that the CytD treatment resulted in TNT collapse and less prominent cell stretching (Fig 1H, I). These data demonstrate that inhibition of BCR-ABL1 by nilotinib induces the formation of TNTs in a manner dependent upon actin polymerization.

Expression of BCR-ABL1 results in reduced TNT formation and cell adhesion

To further study the role of BCR-ABL1 in TNT formation doxycycline inducible BCR-ABL1 (Klucher et al, 1998) (p210) was introduced in Ba/F3 cells. Ba/F3 cells represent a well explored system for characterization of the oncogene function of BCR-ABL1, where expression of BCR-ABL1 allow Ba/F3 cells to grow IL-3 independent (Daley & Baltimore, 1988). The induction of BCR-ABL1 expression by doxycycline was verified by immunoblotting (Fig 2A) and also IL-3-independent growth (Supplementary Fig S2A). BCR-ABL1 induction resulted in more spherical morphology and less firmly fibronectin-attached cells on the coated plastic culture well (Fig 2B). Interestingly, expression of BCR-ABL1 was also accompanied by down-regulation of TNTs (Fig 2C). Conversely, treatment of Kcl-22 cells with nilotinib (100 nM) for 1 h resulted in less spherical cell morphology, increased adherence and TNT formation (Fig 1E, I and 2D). We confirmed inhibition of BCR-ABL1 signaling by imatinib (5 μM) and nilotinib (100 nM) for 24 h, by mass cytometry analysis using phospho-specific antibodies (Gullaksen, Skavland et al., 2017). The level of phosphorylation of CRKL, STAT5 and CREB among others, were all reduced following imatinib and nilotinib treatment in Kcl-22 cells with similar strength of effect between these two inhibitors and thereby not explaining difference in TNT formation (Fig 2E and Supplementary Figure S2B).

TNT formation and increased cell surface adhesion induced by drug treatment

IFNα has previously been shown to induce cell adherence of CML cells by restoring β1 integrin function (Bhatia & Verfaillie, 1998, Dowding et al., 1991). To study the role of cell adherence through β1 integrin in TNT formation, we pre-incubated Kcl-22 cells for 30 min with a blocking antibody against β1 integrin before 1 h treatment with either IFNα (100 U/ml) or nilotinib (100 nM). Kcl-22 cells not pre-incubated with the blocking antibody showed changes in cell morphology and a significant change in cell surface area (μm^2) on fibronectin coated culture

wells following nilotinib treatment, whereas IFNα treatment only resulted in altered morphology without significant changes in cell surface area (Fig 3A-B). Strikingly, these nilotinib and IFNα-induced changes in cell morphology were completely blocked by pre-incubation with the β1 integrin blocking antibody (Fig 3C-D). When measuring cell motility by time-lapse microscopy, we found that the IFNα and nilotinib-induced change in cell morphology was associated with a significant decrease in cell motility. Conversely, pre-treatment with the β1 blocking antibody resulted in increased cell motility (Figure 3C-D) suggesting a direct connection between increased functionality of integrin β1 and cell adherence, here induced by IFNα and nilotinib; and TNT formation.

K562 and Kcl-22 cell lines show different GTPase profiles

Cell adherence and motility can be regulated by the Rho family of small GTPases, including Rac1, Rho and Cdc42 (Keely, Westwick et al., 1997). Cdc42 and Rac1 have both been suggested to play important roles in TNT biogenesis in macrophages (Hanna, McCoy-Simandle et al., 2017, Hase, Kimura et al., 2009). We therefore examined the involvement and activity of these GTPases in cell adherence and TNT formation following nilotinib treatment (100 nM 1h) by GTPase pull-down assays. We found that the total Rac1 protein was weakly expressed in K562 cells with undetectable levels of the active form, whereas the Kcl-22 cells showed higher total expression and activity of Rac1 (Fig 4A). Compared to Kcl-22 cells, K562 cells showed higher expression and activity of Rho and higher activity of Cdc42 (Fig 4 B and C). However, treatments with nilotinib did not result in any major changes in total protein expression or in the activity of these GTPases (Fig 4A-C). These data indicate that formation of TNTs is not dependent upon the activity of the investigated Rho family GTPases. Still, the differences in expression and activity of these proteins at basal level between the two cell lines might explain

some of the differences in their TNT-response after BCR-ABL1 inhibition. Treatment with imatinib or nilotinib caused reduction in the total expression of the Rac1 guanine exchange factor (GEF) protein Tiam-1 in the Kcl-22 cells, which was not observed in the K562 cells (Fig 4D). To further investigate the relation between TNT formation and Rac1 we examined the BCR-ABL1 negative AML cell line HL-60 which expressed high levels of Rac1 and low levels of TNTs (Omsland et al., 2017). HL-60 cells treated with nilotinib (100 nM, 24 h) showed no TNT induction (Figure 4E). These results indicate an involvement of BCR-ABL1 in nilotinib-induced TNT formation in Kcl-22 cells.

Nilotinib-induced TNT formation in CML cells is blocked by co-culture with human derived mesenchymal stromal cells

The interaction between mesenchymal stromal cells (MSCs) and CML cells is important for disease etiology, particularly in modulation of drug sensitivity (Weisberg & Griffin, 2012). We hypothesized that the contact between CML cells and stroma cells might affect formation of TNTs. Therefore, we seeded Kcl-22 cells on a layer of MSC-derived SAOS-2 cells (osteosarcoma cell line) or on human-derived primary healthy MSCs and analyzed TNT formation between CML cells in response to nilotinib. Co-culturing demonstrated near complete blockage of TNT formation in the Kcl-22 cells (Fig 5A and data not shown). To further investigate if this inhibitory effect on TNT formation was dependent on physical contact between the CML cells and stromal cells, we incubated the Kcl-22 cells in conditioned medium from the human-derived MSCs and this resulted in inhibition of TNT-induction by nilotinib (Fig 5B). This suggested the existence of common factors secreted from SAOS-2 cells and MSCs inhibiting TNT formation between CML cells. Two common factors secreted by SAOS-2 and MSCs both in

mono-culture and in co-culture with leukemic cells are CXCL8 (interleukin-8) and vascular endothelial growth factor (VEGF) (Bruserud, Tronstad et al., 2005, Polak et al., 2015).

This prompted us to treat Kcl-22 cells with CXCL8 (20 ng/ml, 24 h) or VEGF (20 ng/ml, 24 h) alone or together with nilotinib (100 nM, 24 h). No change in TNTs was found after treatment with CXCL8 alone, however, co-treatment with CXCL8 and nilotinib resulted in reduced TNT formation compared to nilotinib treatment alone (Figure 5C). In contrast, co-treatment with VEGF and nilotinib resulted in increased TNT formation (Fig 5D). Interestingly, when we measured the concentration of CXCL8 in the cell supernatants of Kcl-22 cells by ELISA, we found a reduced CXCL8 concentration after treatment with nilotinib (100 nM) for 24 h (Fig 5E). This CXCL8 reducing effect by nilotinib has previously been reported in nilotinib-treated patients who showed reduced CXCL8 plasma concentrations (Hantschel, Gstoettenbauer et al., 2008). However, when Kcl-22 cells were co-cultured with SAOS-2 cells an increase in CXCL8 was found in the cell supernatants in nilotinib-treated co-cultures compared to control. No further difference in CXCL8 levels was measured following nilotinib treatment if CXCL8 was added to the Kcl-22 cells alone (Fig 5F). This suggests that an excess of CXCL8 will counteract the TNT-inducing effect of nilotinib. Furthermore, flow cytometry analysis revealed that only the Kcl-22 cells expressed the CXCL8 receptor CXCR2 (Fig 5G). We further verified the importance of CXCL8 in TNT formation by treating the Kcl-22 cells with antibodies against CXCL8 and by blocking the CXCR2 receptor by treatment with reparixin. A slight increase of TNTs was observed after 24 h treatment with 0.2 µg/ml and 0.4 µg/ml CXCL8 blocking antibody or reparixin (1, 10 and 100 nM for 24 h) (Fig 5H and I), but no dramatic change in cell morphology was observed (Supplementary figure 3 A and B). Taken together these results suggests that an intact CXCL8 signaling pathway in the Kcl-22 cells could be part of the observed TNT

modulation following nilotinib treatment, but and inhibition of the CXCL8 pathway alone is not sufficient for a significant induction of TNTs.

Differentiation of Kcl-22 cells by ATRA increases CXCL8 secretion inhibiting the TNT-induction by nilotinib

All-trans retinoic acid (ATRA) differentiate leukemic blast cells to mature myeloid cells (Collins, Gallo et al., 1977) and influence NF-κB regulation and CXCL8 production (Dai, Yamasaki et al., 2004). To further investigate the connection between CXCL8 and TNT formation, Kcl-22 cells were treated for five consecutive days with ATRA (1 µM) to induce differentiation followed by 24 h treatment with nilotinib (100 nM). Interestingly, pre-treatment with ATRA completely prevented nilotinib-induced TNT formation (Fig 6A). Indeed, the concentration of CXCL8 was increased in the cell supernatant of the Kcl-22 cells following incubation with ATRA, whereas nilotinib treatment resulted in a reduction of CXCL8 comparable to untreated Kcl-22 cells (Fig 6B). Although the ATRA-treatment resulted in 30% differentiation of the Kcl-22 cells after May-Grünwald Giemsa staining (Fig 6C and D), no change in cell surface CXCR2 expression was found by flow cytometry analysis (Figure 6E). Together, these data indicate that ATRA treatment may prevent formation of TNTs by increasing signaling through an autocrine CXCL8-CXCR2 pathway.

Discussion

TNT is a dynamic 50-200 nm structure consisting of plasma membrane and F-actin, but with elusive regulatory mechanisms (Zaccard, Rinaldo et al., 2016). Since the BCR-ABL1 fusion protein in CML has a strong impact on F-actin and simultaneously affects various signaling pathways (Van Etten, Jackson et al., 1994) we examined the effect of BCR-ABL1 on TNT formation. Both bone marrow derived BCR-ABL1 positive cells from CML patients and cell lines displayed low numbers of TNTs compared to acute myeloid leukemia cells and other cancer cells (Hase et al., 2009, Omsland et al., 2017, Reichert et al., 2016). A possible explanation for the low TNT numbers could include the observation that CML cells adhere poorly to the bone marrow stroma (Gordon et al., 1987), consequently resulting in interrupted cellular TNT communication. TNT formation between cells *in vitro* is highly dependent on adherence, and culturing leukocytes on a supportive layer of mesenchymal stem cells (MSCs) or fibronectin increase TNT formation (Osteikoetxea-Molnar, Szabo-Meleg et al., 2016, Reichert et al., 2016). IFNα was the first effective CML therapy and is now being re-evaluated in combination with TKIs like dasatinib (Apperley, 2015, Hjorth-Hansen et al., 2016). Interestingly, one of the proposed mechanisms for the efficacy of IFNα in treatment of CML patients was through its ability to restore adhesion of CML cells to the bone marrow stroma (Dowding, Gordon et al., 1993). Similarly, TKI treatments result in increased CML cell adherence to fibronectin (Obr et al., 2014). Together, these observations suggest that restoration of adherence in CML cells could be central to successful treatment of CML patients.

Interestingly, both increased adhesion and change in morphology was observed in the two CML cell lines after imatinib treatment, accompanied by a significant increase in TNT formation. However, treatment with nilotinib as well as IFNα induced adhesion and TNT formation in Kcl-

22 cells, but not in K562 cells (Fig 1B, D and Fig 3A). Evidence for an involvement of BCR-ABL1 in TNT formation was obtained using the doxycycline-inducible system of BCR-ABL1 expression in the Ba/F3 cells. BCR-ABL1 induction caused these cells to appear more morphologically spherical compared to the Ba/F3 control cells (Figure 2D). This confirmed observations by others where BCR-ABL1 expression in Ba/F3 cells induced cell detachment, and increased motility (Salgia, Li et al., 1997).

To verify the importance of cell adhesion in TNT induction we incubated Kcl-22 cells with an integrin β1 blocking antibody before treatment with IFNα or nilotinib. Indeed, we found that the cell adhesion effect by the two therapeutics were dependent of β1 integrin (Fig 3C). The Kcl-22 cells showed increased mobility and a more spherical shape after pre-incubation with the integrin β1 blocking antibody (Fig 3D). Together with the results obtained in the Ba/F3 cell model system, this supports a hypothesis where these CML cells form few TNT structures when adhering poorly to fibronectin as a consequence of showing a spherical appearance.

The RhoGTPases are known to have an impact on F-actin and cell mobility, and also to be implicated in BCR-ABL1 dependent CML leukemogenesis (Harnois, Constantin et al., 2003). It was therefore of interest to investigate the GTPase activity in K562 and Kcl-22 cells. We were unable to demonstrate active Rac1 in the K562 cells in contrast to the Kcl-22 cells where Rac1 was slightly down-regulated Rac1 after nilotinib treatment (Fig 4A). Even though the HL-60 cell line express high levels of Rac1, no induction of TNTs or any increase in cell adhesion was observed after nilotinib treatment in these cells (Figure 4E) suggesting that nilotinib-induced TNT formation could be dependent on the BCR/ABL1/Rac1 pathway. The observed difference in the basal Rho GTPase profiles in these two CML cell lines could represent part of the explanation for the difference in TNT-induction caused by niltoinib and IFNα.

Intercellular communication between leukemic cells and bone marrow stromal cells have a major impact on the leukemic cells (Paraguassu-Braga, Borojevic et al., 2003). Therefore, we investigated if nilotinib treatment also induced TNTs in CML cells in co-culture with stromal cells or the MSC-derived osteosarcoma cell line SAOS-2. Interestingly, the TNT inducing effect was abolished when Kcl-22 cells were seeded on a confluent layer of the osteosarcoma cell line SAOS-2 (Fig 5A) or when incubated in conditioned medium from MSCs (Fig 5B). This observation suggests that common extracellular secreted factors from these cells are inhibiting the nilotinib induced TNT formation. Cytokines have previously been suggested to have an effect on TNT formation in natural killer (NK) cells (Chauveau et al., 2010) and the cytokine CXCL8 as well as the growth factor VEGF are both secreted by both SAOS-2 and healthy bone marrow stromal cells (Bruserud et al., 2005, Polak et al., 2015). When the Kcl-22 cells were incubated with CXCL8 or VEGF together with nilotinib treatment, CXCL8, but not VEGF, inhibited the nilotinib-induced TNT formation (Fig 5C, D).

Multiple studies have demonstrated the pro-survival properties of CXCL8 on CML cells, and also that the CML cells themselves can release CXCL8 (Corrado, Raimondo et al., 2014). In addition, CML cells release exosomes that in turn can induce CXCL8 production and extracellular secretion from the bone marrow stroma cells resulting in increased survival of CML cells (Corrado et al., 2014). Previously, a reduction of CXCL8 in the serum of CML patients treated with imatinib has been demonstrated and dasatinib and nilotinib treatment of K562 cells caused down-regulated CXCL8 gene expression and secretion by the K562 cells (Hantschel et al., 2008). Here we report low levels of CXCL8 secretion by Kcl-22 cells, that was further decreased following nilotinib treatment (Fig 5E) (Hantschel et al., 2008). When CXCL8 concentrations were increased in the cell supernatant of the Kcl-22 cells, either by culturing with SAOS-2 cells

or by adding excess CXCL8 to the Kcl-22 monoculture, the TNT-inducing effect of nilotinib was abolished (Fig 6A, C). This suggests an involvement of CXCL8 in TNT biogenesis. Further support of this involvement is the expression of CXCR2 on the cell surface of Kcl-22 cells, but not in K562 cells, suggesting a potential autocrine-loop that merits further investigation.

All-trans retinoic acid (ATRA) has been shown to induce CXCL8 production in human keratinocytes to expression of functional CXCL8 receptors on HL-60 cells (Dai et al., 2004, Sham, Phatak et al., 1995). We investigated if CXCL8 was increased in the cell supernatant of Kcl-22 cells after treatment with ATRA and the effect of increased CXCL8 production on TNT formation by treating Kcl-22 with ATRA. When Kcl-22 cells were treated with ATRA for five days the CXCL8 concentration in the cell supernatant was increased compared to untreated control cells and subsequently treatment with nilotinib for 24 h resulted in reduction of CXCL8 (Fig 6B). Approximately 30% of the Kcl-22 cells differentiated to neutrophil granulocytes as determined by May-Grünwald staining (Fig 6C and D), but the total surface CXCR2 expression remained unchanged (Fig 6E).

Taken together, we find that imatinib treatment induces TNT formation in the CML cell lines Kcl-22 and K562. TNTs were induced in Kcl-22 cells, but not K562 cells, following IFNα and nilotinib treatment. We propose that TNT induction caused by IFNα and nilotinib is correlated to increased cell adhesion involving β1-integrin, potentially also including the BCR-ABL1/CXCL8 pathway (Fig 7). The functional consequences of TNT induction needs to be further investigated.

Materials and Methods

Cell lines

K562, Kcl-22 and Ba/F3 cells (ATCC and DSMZ) were cultured according to provider's instructions. RPMI-1640 medium was supplemented with 10% FBS, 1% L-glutamine (2mM) and 1% (1.0 U/ml) penicillin and streptomycin (5mM) (Sigma-Aldrich). The RPMI-1640 medium for the IL-3 dependent Ba/F3 cells were additionally supplemented with 10% conditioned medium from WEHI3B cells (mouse myelomonocytic cell line) known to secrete high amounts of IL-3 (Lee, Hapel et al., 1982). The WEHI3B cells were grown to confluency in a T75 flask with complete IMDM medium (containing 10 % FBS, 1 % Pen-Strep and L-glutamine), and cultured for 2-3 days before the supernatant was centrifuged at 1500 RPM for 10 min and sterile filtered through a 0.2 µm filter.

Mem-GFP transduced cells

The memGFP-Kcl-22 and mem-GFP-K562 cells were generated by transducing the cells with ready-to-use lentiviral particles expressing a membrane localization signal (20 amino acids of the N-terminal part of neuromodulin, containing a palmitolylation signal) fused to GFP; rLV-EF1-AcGFP-Mem-9 (Takara, rV2.1A1.1941 C2) according to the provider's instructions. The transduced cells were sorted using BD FACS Aria SORP at the Flow Cytometry Core Facility, Department of Clinical Science, University of Bergen, Norway.

Primary cells

The study was conducted in accordance with the Declaration of Helsinki and approved by the local Ethics Committee (Regional Ethics Committee West projects 2012/2245 and 2012/2247,

University of Bergen, Norway). Blood and bone marrow samples from consecutively diagnosed CML patients were collected after informed consent and were processed by density gradient separation (Lymphoprep, Axis-Shield, Oslo, Norway) (Bruserud, Gjertsen et al., 2001).

Doxycycline inducible Ba/F3 cells

BCR-ABL1 (P210) was cloned into pcDNA3 (Adgene) after EcoRI digestion. The orientation and sequence was verified by PCR. This was further sub-cloned into the EcoRI site of PLVX-tetOne-Puro (from the Lenti-X Tet-One Inducible Expression Systems). Wild type Ba/F3 (kind gift to Prof. Enserink from Prof. Gordon Mills laboratory, Houston, Texas, USA) was transfected with 2 µg of the PLVX_tetOne_BCR-ABL1 plasmid or PLVX_tetOne_empty vector by electroporation (Amaxa biosystems nucleofector II: program U20) using Ingenio Electroporation solution (catalog number MIR 50114). Transfected cells were cultured in medium for 24-72 h before selection with 1 µg/ml puromycin. Puromycin resistant clones were sorted and grown independently; cells were continually cultured in medium with puromycin to maintain selection pressure. 0.1 µg/ml doxycycline was added to induce expression of BCR-ABL1.

Antibodies and reagents

The following primary antibodies were used for immunofluorescence and/or immunoblotting: anti-β-tubulin (clone TUB 2.1, Sigma-Aldrich), anti-COX IV (ab16056), anti-GAPDH (ab9485, abcam) anti-cAbl ((24-11) sc-23, Santa Cruz Biotechnology), Tiam-1 (C-16, sc-872, Santa Cruz Biotechnology), anti-integrin β1 blocking antibody [P5D2] (ab24693, Abcam), anti-Rac1 (from active Rac-1 pull-down and detection kit cat#16118, ThermoFischerScientific), anti-Cdc42 (from active Cdc42 pull-down and detection kit cat#16119, ThermoFischerScientific) and anti-Rho

(detecting RhoA, RhoB and RhoC), (from active Rho pull-down and detection kit cat#16116, ThermoFischerScientific). Secondary antibodies used for immunofluorescence or immunoblotting; Alexa Fluor© 488- or 594-conjugated goat-anti-mouse (Invitrogen), horseradish peroxidase (HRP)-conjugated goat anti-rabbit/mouse (Jackson Immunoresearch). The following were used for actin and membrane staining; AlexaFluor© 350-conjugated phalloidin and wheat germ agglutinin (WGA) –Alexa Fluor© 594 or 488 (Invitrogen) as previously described (Omsland et al., 2017). Tyrosine kinase inhibitors: Imatinib and Nilotinib (Selleckchem). Interferon alpha (IFNα) (Intron A from MSD), Cytochalasin D (Sigma-Aldrich), doxycycline (Doxyferm, Nordic Drugs AB, Limhamn), puromycin (Sigma-Aldrich), May-Grünwald (Merck KgaA), Giemsa (Merck KgaA), Sören phosphate buffer (Hospital Pharmacy Haukeland University Hospital), Bovine serum albumin (BSA) fraction V (Roche), All-trans retinoic acid (ATRA) (Sigma-Aldrich), fibronectin (Sigma-Aldrich), anti-CXCL8 (R&D systems) and reparixin (Cayman chemical).

TNT identification and quantification

A TNT in this study is defined as a thin straight structure, ≤ 200 nm in diameter, minimum 5 µm in length, hovering above the substratum, connecting two cells. TNTs were distinguished from cytoplasmic bridges, which appear following cell division, by the lack of a midbody clearly visible by differential interference contrast and/or staining of cellular membranes (Omsland et al., 2017). 8-well µ-slides (Ibidi GmbH) were pre-coated with fibronectin (10 µg/ml, F2006, Sigma-Aldrich) for 30 min at 37°C before washing with saline. 70000 cells were seeded per well and incubated overnight under physiological conditions. Primary CML cells were seeded in DMEM medium containing 20% FBS overnight and stained with wheat germ agglutinin conjugated with alexa fluor 488 or 594 (1.67 µg/ml) as previously described (Omsland et al., 2017). Cells were

399 examined live by fluorescent light microscopy (Zeiss Axio Observer Z1 with AxioVision 4.8.2 or
400 Zen software) using a 63X/1.4 NA Oil DICIII objective, heat block (37°C) and standard air
401 conditions. 100 cells per well were counted following a fixed counting pattern with 5-6 cells
402 examined per vision field. The result is described as number of TNTs/100 cells meaning the total
403 number of TNTs (one TNT always connects two cells) among 100 cells counted. For further
404 details see Supplementary Figure in Omsland et al (Omsland et al., 2017). Cell viability was
405 monitored by Hoechst 3342 (Sigma) staining as previously described (McCormack, Haaland et
406 al., 2012).
407
408 **Blocking of integrin β-1**
409 Cells were cultured in a $0.7x10^6$ cells/ml density in a 6-well plate. Cells were incubated in
410 medium without or with 10 µg/ml of anti-integrin beta 1 [P5D2] antibody for 30 min before
411 seeded to fibronectin pre-coated µ-slides (Ibidi GmbH). Cells were incubated for 3 h to allow
412 attachment before treatment with 1 µM nilotinib (nilo) or 100 U/ml IFNα 1 h prior to
413 examination by live microscopy.
414 Measuring of cell area was performed manually using ImageJ: Images were analyzed as 8-bit
415 files using FFT Bandpass Filter, threshold was set manually and adjusted until cells were
416 distinguished from the background>convert to mask>fill holes>cells in close proximity were then
417 distinguished using watershed algorithm. Measuring of the cell area was performed using the
418 measure tool under the region of interest manager tool and single cells were selected using the
419 wand tool.
420 Tracking of cells was performed using metamorph and the chemotaxis and migration (Ibidi
421 GmbH) plugin to ImageJ was performed to calculate accumulated distance and to make trajectory
422 plots as described in (Hurley, Smith et al., 2013).

423

424 **Immunofluorescence**

425 The F-actin and microtubule presence in TNTs was investigated in Kcl-22 cells (on 8-well μ-
426 slides, Ibidi GmbH) fixed in 4% PFA in PBS and 0.2% glutaraldehyde in PBS for 20 min at room
427 temperature (RT) followed by one wash with PBS, before permeabilized for 1 min using 0.2%
428 Tween© in PBS and washed twice with PBS. Cells were blocked with 0.5% Bovine Serum
429 Albumin Fraction V (BSA) PBS for 20 min at RT and then incubated for 1 h at RT in the dark
430 with 33nM AlexaFluor© phalloidin, washed once with PBS and incubated with anti-β-tubulin
431 antibody (1:200 in blocking solution) overnight at 4°C. Then cells were washed twice with PBS
432 and incubated with Alexa-488 or 594 goat-anti-mouse antibodies (1:5000 in blocking solution)
433 for 1h at RT, before washed twice with PBS and examined by fluorescence microscopy. Cells not
434 expressing memGFP were stained with wheat germ agglutinin (WGA) conjugated with Alexa
435 488 or 594 for 8 min followed by one wash with PBS before examined by microscopy and
436 manual quantification of TNTs.

437

438 **Scanning electron microscopy (SEM)**

439 500 0000 cells were seeded on L-lysine pre-coated coverslips followed by incubation at 37°C
440 overnight before fixed (4 % glutaraldehyde in 0.2 M Na-cacodylate in buffer diluted 1:1 with
441 medium) for 2 h at RT. Cells were carefully washed three times for 15 min using 0.1 M Na-
442 cacodylate buffer followed by 60 min post-fixation with 1% osmiumtetraoxide in 0.1 M Na-
443 cacodylate buffer and washed twice for 10 min with 0.1 M Na-cacodylate buffer. Dehydration
444 was performed with 30 % ethanol for 15 min, 50 % ethanol for 15 min, 70 % ethanol for 20 min
445 or overnight, 96 % ethanol for 20 min and twice with 100 % ethanol for 20 min. The coverslips

were obtained from the wells and placed on SEM stubs before incubated in a heat-incubator overnight. Critical point drying was omitted in order to avoid breakage of TNTs. The SEM stubs were coated with 5-10 nm gold/palladium before analyzed by SEM microscopy.

Immunoblotting

Cells were lysed and analyzed by immunoblotting according to standard protocol (Shieh, Taya et al., 1999, Silden, Hjelle et al., 2013). Briefly, immunobloting was performed using precast gels from BioRad, transferred to PVDF membranes using Pierce G2 fast blotter (Thermo Scientific). Membranes were blocked for 1h at RT in 5% fat-free drymilk or 3% BSA in TBST, incubated with primary antibody at 4°C overnight. Membranes were washed with TBST followed by incubation for 1 h with secondary antibody ((HRP)-conjugated goat-anti-rabbit/mouse) was diluted 1:1000 in 5% drymilk in TBST and washed with TBST before developed using SuperSignal West pico or femto (Thermo Fisher Scientific). Developed immunoblots were detected and captured by ImageQuant LAS 4000 (GE Healthcare Life Sciences). Quantification of immunoblot bands were performed on 16-bit original files using 1D gel analysis option in ImageQuant TL version 8.1 (GE healthcare). Lane creation was performed with the manual option and background was subtracted using the manual baseline option in this program. The final value after background subtraction was used for calculating the ratio relative to the loading control.

RhoGTPase activity assays

All RhoGTPase assays were performed according to the manufacture protocol of the individual GTPase pulldown activity assays used (ThermoFischerScientific). Briefly, $10x10^6$ cells were treated with 100 nM nilotinib for 1 h before washed and lysed in lysis/wash buffer with protease

inhibitors, incubated on ice for 10 min before centrifugation at 12 000 x g for 15 min. Protein concentration was measured using the Bradford Assay. GTPγS was used as a positive control and GDP as a negative control. In each reaction 500 µg cell lysates were used added 10 mM EDTA and 0.1 mM GTPγS or GDP followed by incubation at 30°C for 15 min with shaking (300RPM). The reaction was stopped by adding 60 mM $MgCl_2$ on ice. The pull-down was performed with 500-1000 µg cell lysate. For pull-down of active Rho, 400 µg GST-Rhotektin-PBD together with gluthation resin was used, for Rac1 and Cdc42 20 µg GST-PAK1-PBD was used. Fresh β-mercaptoethanol was added to the 2x sample buffer included in the kit. Regular immunoblotting was performed as earlier described, where 28 µl of the eluted samples were applied to gels.

Flow cytometry

$0.5x10^6$ cells were centrifuged for 5 min, 200 RCF at 4°C, washed once with saline, centrifuge and blocked in 0.5% BSA in PBS for 15 min on ice. Cells were incubated with primary antibody CXCR2 (0.5 µg/ml final concentration) for 30 min on ice, washed twice with blocking solution and incubated with secondary antibody (goat-anti mouse alexa-fluor-647) for 20 min on ice, before washed twice and analyzed using Guava easy cyte™ (Millipore) flow cytometer by the Guava Soft version 2.2.2 software. Flow cytometry results were analyzed using FlowJo 10.1 (Treestar).

All-trans retinoic acid (ATRA) treatment and differentiation

$2x10^6$ cells were seeded in 25 cm^3 flasks with medium only or 1 µM ATRA. All experiments including ATRA were performed protected from light exposure. After three days of incubation the cells were centrifuged and resuspended in freshly made medium with or without ATRA and incubated for additional 48 h. $1x10^6$ cells were used for preparation of supernatants for ELISA

494 analysis, microscopy and flow cytometry. The remaining were seeded onto a 6-well plate and
495 incubated with or without 100 nM nilotinib for 24 h following lysis and fixation for western blot
496 analysis and mass cytometry, respectively.
497
498 **May-Grünwald Giemsa staining**
499 Cells were cytospun 4 min, 400 RPM, air-dried and cells were circled using a PAP-pen. Cells
500 were fixed by incubation for 20 min in methanol and further stained with freshly made May-
501 Grünwald solution diluted 1:1 in Sörens phosphate buffer for 15 min at RT followed by Giemsa
502 staining (diluted 1:10 in Sörens phosphate buffer) for 5 min before washing in Sörens phosphate
503 buffer. Cells were air dried before examined by bright field microscopy.
504
505 **ELISA**
506 A human CXCL8 quantikine sandwich ELISA (R&D systems) was performed according to the
507 manufacture's protocol. Supernatants were collected from the µ-wells (Ibidi GmbH) after TNT
508 quantification for the co-cultures and CXCL8 supplemented in the medium of Kcl-22 cells. To be
509 able to detect CXCL8 values in control samples of Kcl-22 cells, $1x10^6$ cells were incubated with
510 or without 100 nM nilotinib for 24 h. For the ATRA pre-treated cells and untreated controls, the
511 cells were collected at day 5, centrifuged and prepared for nilotinib treatement as described
512 above.
513
514 **Mass Cytometry**
515 **Barcoding**

To reduce experiment variability, workload and antibody consumption, we used the commercially available metal barcoding kit from Fluidigm. Briefly, the cells from each sample were stained with a unique three-palladium isotope combination; three chosen from six available; Pd 102, Pd 104, Pd 105, Pd 106, Pd 108, Pd 110 (20 unique combinations available). After cell barcoding and washing according to the manufacturers' recommendations, uniquely barcoded samples were pooled for further processing for mass cytometry analysis.

Antibody staining

A pool of barcoded cells was stained with a panel of cell surface markers (30 minutes, RT) and permeabilized with methanol (-20^{o}C). Further staining with intracellular phospho-specific antibodies (30 minutes, RT) followed. Cells were then washed and re-suspended in the buffer containing Iridium-intercalator (natural abundance iridium as pentamethylcyclopentadienyl-Iridium (III)-dipyridophenazine), which intercalates into the DNA (1 hour, 4^{o}C), before washed and pelleted by centrifugation. Immediately prior to data acquisition cells were re-suspended to a final concentration of approximately 5x10^{5} cells/mL in MaxPar water (Fluidigm) containing normalization beads (1:10 dilution, Fluidigm) and analyzed on a Helios mass cytometer (Fluidigm), placed in the Flow Cytometry Core Facility of Bergen, University of Bergen.

Single cell discrimination and barcoding de-convolution

Using the normalization beads and the normalization software, any drift in the data resulting from loss of detector sensitivity was abrogated. An automatic barcode deconvolution algorithm developed by Zunder *et al* 2015 (Zunder, Finck et al., 2015) was used to identify each uniquely barcoded sample. Further discrimination and gating of single cells was achieved by plotting all events by DNA-content (Ir 191 or Ir 103) versus Event Length (number of pushes). Together,

barcode deconvolution and gating of cells on DNA content versus event length, is an effective filter for removal of doublets and identification of single cells. Finally, cleaved Caspase 3 readily discriminated between apoptotic and non-apoptotic cells, where non-apoptotic cells were used for statistical analysis.

Table 1 Antibody panel for mass cytometry analysis

A.m.u	Metal	Epitope	Clone	Vendor
102	Pd	Metal Barcode Channel #1	N.A.	Fluidigm
104	Pd	Metal Barcode Channel #2	N.A.	Fluidigm
105	Pd	Metal Barcode Channel #3	N.A.	Fluidigm
106	Pd	Metal Barcode Channel #4	N.A.	Fluidigm
108	Pd	Metal Barcode Channel #5	N.A.	Fluidigm
110	Pd	Metal Barcode Channel #6	N.A.	Fluidigm
89	Y	CD45	HI30	Fluidigm
141	Pr	pBCR Y177	Polyclonal	Cell Signaling Technologies
142	Nd	Caspase 3 Cleaved	D3E9	Fluidigm
143	Nd	pCrkL [Y207]	Polyclonal	Fluidigm
149	Sm	p4E-BP1	236B4	Fluidigm
150	Nd	pStat5 [Y694]	47	Fluidigm
153	Eu	pStat1 [Y701]	58D6	Fluidigm
154	Sm	pAbl Y245	73E5	Cell Signaling Technologies
156	Gd	p-p38 [T180/Y182]	D3F9	Fluidigm
158	Gd	pStat3 [Y705]	4/P-STAT3	Fluidigm
165	Ho	pCREB [S133]	4/P-STAT3	Fluidigm
167	Yb	pERK 1/2 [T202/Y204]	D1314.4E	Fluidigm
172	Yb	pS6 [S235/S236]	N7-548	Fluidigm
176	Yb	pS6 [S240/S244]	D68F8	Cell Signaling Technologies
191	Ir	DNA	N.A.	Fluidigm
193ß	Ir	DNA	N.A.	Fluidigm

Statistical analysis

Differences between two groups were analyzed by two-tailed unpaired T-test using GraphPad Prism 6 Version 6.03. F-test was performed to verify that the internal variance in the groups were not significant. Significant difference was considered by a P-value <0.05. For cell area and cell movement unpaired Mann Whitney tests were performed.

Acknowledgments

The confocal and SEM imaging was performed at the Molecular Imaging Center, Department of Biomedicine, University of Bergen. We thank Dr. André Sulen for help with sorting the K562-mem-GFP and Kcl-22-mem-GFP cells and Calum Leitch and Dr. Genoveffa Franchini for helpful feedback on the manuscript. We thank Dr. Tatiana Karpova for assistance with the analysis of cell movement.

Author contributions

MO: was involved in designing the study, performed the experiments, analyzed the data and wrote paper, VA, designed study, performed experiments, analyzed the data and wrote the paper, BTG: designed study, analyzed data and wrote the paper. SEG performed mass spectrometry experiments, MPAD generated the BCR-ABL1 doxycycline inducible Ba/F3 cells and wrote the paper, JE provided cell lines and wrote the paper. RH diagnosed CML patients and verified CML cell lines and wrote paper.

Conflict-of-interest

The authors declare no conflict of interest.

Funding

This study was supported by University of Bergen (MO), Norwegian Cancer Society with Solveig & Ole Lunds Legacy (BTG) and Øyvinn Mølbach-Petersens Fond for Clinical Research (BTG; (Grant no. 104712, 145268, 145269 and 163424) and Bergen Research Foundation (VA).

References

Ahmad T, Mukherjee S, Pattnaik B, Kumar M, Singh S, Kumar M, Rehman R, Tiwari BK, Jha KA, Barhanpurkar AP, Wani MR, Roy SS, Mabalirajan U, Ghosh B, Agrawal A (2014) Miro1 regulates intercellular mitochondrial transport & enhances mesenchymal stem cell rescue efficacy. *Embo J* 33: 994-1010

Andresen V, Wang X, Ghimire S, Omsland M, Gjertsen BT, Gerdes HH (2013) Tunneling nanotube (TNT) formation is independent of p53 expression. *Cell Death Differ* 20: 1124

Apperley JF (2015) Chronic myeloid leukaemia. *Lancet* 385: 1447-59

Bhatia R, McGlave PB, Dewald GW, Blazar BR, Verfaillie CM (1995) Abnormal function of the bone marrow microenvironment in chronic myelogenous leukemia: role of malignant stromal macrophages. *Blood* 85: 3636-45

Bhatia R, Verfaillie CM (1998) Inhibition of BCR-ABL expression with antisense oligodeoxynucleotides restores beta1 integrin-mediated adhesion and proliferation inhibition in chronic myelogenous leukemia hematopoietic progenitors. *Blood* 91: 3414-22

Bruserud O, Gjertsen BT, Foss B, Huang TS (2001) New strategies in the treatment of acute myelogenous leukemia (AML): in vitro culture of aml cells--the present use in experimental studies and the possible importance for future therapeutic approaches. *Stem Cells* 19: 1-11

Bruserud O, Tronstad KJ, Berge R (2005) In vitro culture of human osteosarcoma cell lines: a comparison of functional characteristics for cell lines cultured in medium without and with fetal calf serum. *J Cancer Res Clin Oncol* 131: 377-84

Casella JF, Flanagan MD, Lin S (1981) Cytochalasin D inhibits actin polymerization and induces depolymerization of actin filaments formed during platelet shape change. *Nature* 293: 302-5

Chauveau A, Aucher A, Eissmann P, Vivier E, Davis DM (2010) Membrane nanotubes facilitate long-distance interactions between natural killer cells and target cells. *Proc Natl Acad Sci U S A* 107: 5545-50

Chinnery HR, Pearlman E, McMenamin PG (2008) Cutting edge: Membrane nanotubes in vivo: a feature of MHC class II+ cells in the mouse cornea. *J Immunol* 180: 5779-83

Collins SJ, Gallo RC, Gallagher RE (1977) Continuous growth and differentiation of human myeloid leukaemic cells in suspension culture. *Nature* 270: 347-9

Corrado C, Raimondo S, Saieva L, Flugy AM, De Leo G, Alessandro R (2014) Exosome-mediated crosstalk between chronic myelogenous leukemia cells and human bone marrow stromal cells triggers an interleukin 8-dependent survival of leukemia cells. *Cancer Lett* 348: 71-6

Dai X, Yamasaki K, Shirakata Y, Sayama K, Hashimoto K (2004) All-trans-retinoic acid induces interleukin-8 via the nuclear factor-kappaB and p38 mitogen-activated protein kinase pathways in normal human keratinocytes. *J Invest Dermatol* 123: 1078-85

Daley GQ, Baltimore D (1988) Transformation of an interleukin 3-dependent hematopoietic cell line by the chronic myelogenous leukemia-specific P210bcr/abl protein. *Proc Natl Acad Sci U S A* 85: 9312-6

607 Dowding C, Gordon M, Guo AP, Maison D, Osterholz J, Siczkowski M, Goldman J (1993) Potential
608 mechanisms of action of interferon-alpha in CML. *Leuk Lymphoma* 11 Suppl 1: 185-91

609 Dowding C, Guo AP, Osterholz J, Siczkowski M, Goldman J, Gordon M (1991) Interferon-alpha
610 overrides the deficient adhesion of chronic myeloid leukemia primitive progenitor cells to bone marrow
611 stromal cells. *Blood* 78: 499-505

612 Druker BJ, Tamura S, Buchdunger E, Ohno S, Segal GM, Fanning S, Zimmermann J, Lydon NB (1996)
613 Effects of a selective inhibitor of the Abl tyrosine kinase on the growth of Bcr-Abl positive cells. *Nat Med*
614 2: 561-6

615 Gordon MY, Dowding CR, Riley GP, Goldman JM, Greaves MF (1987) Altered adhesive interactions
616 with marrow stroma of haematopoietic progenitor cells in chronic myeloid leukaemia. *Nature* 328: 342-4

617 Gullaksen SE, Skavland J, Gavasso S, Tosevski V, Warzocha K, Dumrese C, Ferrant A, Gedde-Dahl T,
618 Hellmann A, Janssen J, Labar B, Lang A, Majeed W, Mihaylov G, Stentoft J, Stenke L, Thaler J, Thielen
619 N, Verhoef G, Voglova J et al. (2017) Single cell immune profiling by mass cytometry of newly
620 diagnosed chronic phase chronic myeloid leukemia treated with nilotinib. *Haematologica* 102: 1361-1367

621 Gurke S, Barroso JF, Hodneland E, Bukoreshtliev NV, Schlicker O, Gerdes HH (2008) Tunneling
622 nanotube (TNT)-like structures facilitate a constitutive, actomyosin-dependent exchange of endocytic
623 organelles between normal rat kidney cells. *Exp Cell Res* 314: 3669-83

624 Hanna SJ, McCoy-Simandle K, Miskolci V, Guo P, Cammer M, Hodgson L, Cox D (2017) The Role of
625 Rho-GTPases and actin polymerization during Macrophage Tunneling Nanotube Biogenesis. *Sci Rep* 7:
626 8547

627 Hantschel O, Gstoettenbauer A, Colinge J, Kaupe I, Bilban M, Burkard TR, Valent P, Superti-Furga G
628 (2008) The chemokine interleukin-8 and the surface activation protein CD69 are markers for Bcr-Abl
629 activity in chronic myeloid leukemia. *Mol Oncol* 2: 272-81

630 Harnois T, Constantin B, Rioux A, Grenioux E, Kitzis A, Bourmeyster N (2003) Differential interaction
631 and activation of Rho family GTPases by p210bcr-abl and p190bcr-abl. *Oncogene* 22: 6445-54

632 Hase K, Kimura S, Takatsu H, Ohmae M, Kawano S, Kitamura H, Ito M, Watarai H, Hazelett CC,
633 Yeaman C, Ohno H (2009) M-Sec promotes membrane nanotube formation by interacting with Ral and
634 the exocyst complex. *Nat Cell Biol* 11: 1427-32

635 Hjorth-Hansen H, Stentoft J, Richter J, Koskenvesa P, Hoglund M, Dreimane A, Porkka K, Gedde-Dahl
636 T, Gjertsen BT, Gruber FX, Stenke L, Eriksson KM, Markevarn B, Lubking A, Vestergaard H, Udby L,
637 Bjerrum OW, Persson I, Mustjoki S, Olsson-Stromberg U (2016) Safety and efficacy of the combination
638 of pegylated interferon-alpha2b and dasatinib in newly diagnosed chronic-phase chronic myeloid
639 leukemia patients. *Leukemia* 30: 1853-60

640 Hochhaus A, Larson RA, Guilhot F, Radich JP, Branford S, Hughes TP, Baccarani M, Deininger MW,
641 Cervantes F, Fujihara S, Ortmann CE, Menssen HD, Kantarjian H, O'Brien SG, Druker BJ, Investigators I
642 (2017) Long-Term Outcomes of Imatinib Treatment for Chronic Myeloid Leukemia. *N Engl J Med* 376:
643 917-927

644 Hurley A, Smith M, Karpova T, Hasley RB, Belkina N, Shaw S, Balenga N, Druey KM, Nickel E,
645 Packard B, Imamichi H, Hu Z, Follmann D, McNally J, Higgins J, Sneller M, Lane HC, Catalfamo M

(2013) Enhanced effector function of CD8(+) T cells from healthy controls and HIV-infected patients occurs through thrombin activation of protease-activated receptor 1. *J Infect Dis* 207: 638-50

Joyce JA, Pollard JW (2009) Microenvironmental regulation of metastasis. *Nat Rev Cancer* 9: 239-52

Keely PJ, Westwick JK, Whitehead IP, Der CJ, Parise LV (1997) Cdc42 and Rac1 induce integrin-mediated cell motility and invasiveness through PI(3)K. *Nature* 390: 632-6

Lee JC, Hapel AJ, Ihle JN (1982) Constitutive production of a unique lymphokine (IL 3) by the WEHI-3 cell line. *J Immunol* 128: 2393-8

Lou E, Fujisawa S, Morozov A, Barlas A, Romin Y, Dogan Y, Gholami S, Moreira AL, Manova-Todorova K, Moore MA (2012) Tunneling nanotubes provide a unique conduit for intercellular transfer of cellular contents in human malignant pleural mesothelioma. *PLoS One* 7: e33093

Matula Z, Nemeth A, Lorincz P, Szepesi A, Anna B, Buzas EI, Low P, Nemet K, Uher F, Urban V (2016) The role of extracellular vesicle and tunneling nanotube-mediated intercellular cross-talk between mesenchymal stem cells and human peripheral T cells. *Stem Cells Dev*

McCormack E, Haaland I, Venas G, Forthun RB, Huseby S, Gausdal G, Knappskog S, Micklem DR, Lorens JB, Bruserud O, Gjertsen BT (2012) Synergistic induction of p53 mediated apoptosis by valproic acid and nutlin-3 in acute myeloid leukemia. *Leukemia* 26: 910-7

Obr A, Roselova P, Grebenova D, Kuzelova K (2014) Real-time analysis of imatinib- and dasatinib-induced effects on chronic myelogenous leukemia cell interaction with fibronectin. *PLoS One* 9: e107367

Omsland M, Bruserud O, Gjertsen BT, Andresen V (2017) Tunneling nanotube (TNT) formation is downregulated by cytarabine and NF-kappaB inhibition in acute myeloid leukemia (AML). *Oncotarget* 8: 7946-7963

Onfelt B, Nedvetzki S, Yanagi K, Davis DM (2004) Cutting edge: Membrane nanotubes connect immune cells. *J Immunol* 173: 1511-3

Osteikoetxea-Molnar A, Szabo-Meleg E, Toth EA, Oszvald A, Izsepi E, Kremlitzka M, Biri B, Nyitray L, Bozo T, Nemeth P, Kellermayer M, Nyitrai M, Matko J (2016) The growth determinants and transport properties of tunneling nanotube networks between B lymphocytes. *Cell Mol Life Sci* 73: 4531-4545

Paraguassu-Braga FH, Borojevic R, Bouzas LF, Barcinski MA, Bonomo A (2003) Bone marrow stroma inhibits proliferation and apoptosis in leukemic cells through gap junction-mediated cell communication. *Cell Death Differ* 10: 1101-8

Pasquier J, Guerrouahen BS, Al Thawadi H, Ghiabi P, Maleki M, Abu-Kaoud N, Jacob A, Mirshahi M, Galas L, Rafii S, Le Foll F, Rafii A (2013) Preferential transfer of mitochondria from endothelial to cancer cells through tunneling nanotubes modulates chemoresistance. *J Transl Med* 11: 94

Polak R, de Rooij B, Pieters R, den Boer ML (2015) B-cell precursor acute lymphoblastic leukemia cells use tunneling nanotubes to orchestrate their microenvironment. *Blood* 126: 2404-14

Rainy N, Chetrit D, Rouger V, Vernitsky H, Rechavi O, Marguet D, Goldstein I, Ehrlich M, Kloog Y (2013) H-Ras transfers from B to T cells via tunneling nanotubes. *Cell Death Dis* 4: e726

682 Reichert D, Scheinpflug J, Karbanova J, Freund D, Bornhauser M, Corbeil D (2016) Tunneling nanotubes
683 mediate the transfer of stem cell marker CD133 between hematopoietic progenitor cells. *Exp Hematol*

684 Rustom A, Saffrich R, Markovic I, Walther P, Gerdes H-H (2004) Nanotubular highways for intercellular
685 organelle transport. *Science* 303: 1007-10

686 Salgia R, Li JL, Ewaniuk DS, Pear W, Pisick E, Burky SA, Ernst T, Sattler M, Chen LB, Griffin JD
687 (1997) BCR/ABL induces multiple abnormalities of cytoskeletal function. *J Clin Invest* 100: 46-57

688 Seyed-Razavi Y, Hickey MJ, Kuffova L, McMenamin PG, Chinnery HR (2013) Membrane nanotubes in
689 myeloid cells in the adult mouse cornea represent a novel mode of immune cell interaction. *Immunol Cell*
690 *Biol* 91: 89-95

691 Sham RL, Phatak PD, Belanger KA, Packman CH (1995) Functional properties of HL60 cells matured
692 with all-trans-retinoic acid and DMSO: differences in response to interleukin-8 and fMLP. *Leuk Res* 19: 1-
693 6

694 Shieh SY, Taya Y, Prives C (1999) DNA damage-inducible phosphorylation of p53 at N-terminal sites
695 including a novel site, Ser20, requires tetramerization. *EMBO J* 18: 1815-23

696 Silden E, Hjelle SM, Wergeland L, Sulen A, Andresen V, Bourdon JC, Micklem DR, McCormack E,
697 Gjertsen BT (2013) Expression of TP53 isoforms p53beta or p53gamma enhances chemosensitivity in
698 TP53(null) cell lines. *PLoS One* 8: e56276

699 Simonsson B, Gedde-Dahl T, Markevarn B, Remes K, Stentoft J, Almqvist A, Bjoreman M, Flogegard M,
700 Koskenvesa P, Lindblom A, Malm C, Mustjoki S, Myhr-Eriksson K, Ohm L, Rasanen A, Sinisalo M,
701 Sjalander A, Stromberg U, Bjerrum OW, Ehrencrona H et al. (2011) Combination of pegylated IFN-
702 alpha2b with imatinib increases molecular response rates in patients with low- or intermediate-risk chronic
703 myeloid leukemia. *Blood* 118: 3228-35

704 Sowinski S, Jolly C, Berninghausen O, Purbhoo MA, Chauveau A, Kohler K, Oddos S, Eissmann P,
705 Brodsky FM, Hopkins C, Onfelt B, Sattentau Q, Davis DM (2008) Membrane nanotubes physically
706 connect T cells over long distances presenting a novel route for HIV-1 transmission. *Nat Cell Biol* 10:
707 211-9

708 Van Etten RA, Jackson PK, Baltimore D, Sanders MC, Matsudaira PT, Janmey PA (1994) The COOH
709 terminus of the c-Abl tyrosine kinase contains distinct F- and G-actin binding domains with bundling
710 activity. *J Cell Biol* 124: 325-40

711 Verfaillie CM, McCarthy JB, McGlave PB (1992) Mechanisms underlying abnormal trafficking of
712 malignant progenitors in chronic myelogenous leukemia. Decreased adhesion to stroma and fibronectin
713 but increased adhesion to the basement membrane components laminin and collagen type IV. *The Journal*
714 *of clinical investigation* 90: 1232-41

715 Wang X, Gerdes HH (2015) Transfer of mitochondria via tunneling nanotubes rescues apoptotic PC12
716 cells. *Cell Death Differ* 22: 1181-91

717 Weisberg E, Griffin JD (2012) CML cell trafficking: Influence of the stromal microenvironment. *Open*
718 *Journal of Hematology* 3: 1

719 Weisberg E, Manley PW, Breitenstein W, Bruggen J, Cowan-Jacob SW, Ray A, Huntly B, Fabbro D,
720 Fendrich G, Hall-Meyers E, Kung AL, Mestan J, Daley GQ, Callahan L, Catley L, Cavazza C, Azam M,

721 Mohammed A, Neuberg D, Wright RD et al. (2005) Characterization of AMN107, a selective inhibitor of
722 native and mutant Bcr-Abl. *Cancer Cell* 7: 129-41

723 Wertheim JA, Perera SA, Hammer DA, Ren R, Boettiger D, Pear WS (2003) Localization of BCR-ABL to
724 F-actin regulates cell adhesion but does not attenuate CML development. *Blood* 102: 2220-8

725 Zaccard CR, Rinaldo CR, Mailliard RB (2016) Linked in: immunologic membrane nanotube networks. *J*
726 *Leukoc Biol* 100: 81-94

727 Zunder ER, Finck R, Behbehani GK, Amir el AD, Krishnaswamy S, Gonzalez VD, Lorang CG, Bjornson
728 Z, Spitzer MH, Bodenmiller B, Fantl WJ, Pe'er D, Nolan GP (2015) Palladium-based mass tag cell
729 barcoding with a doublet-filtering scheme and single-cell deconvolution algorithm. *Nat Protoc* 10: 316-33

730

731

732

733

734

735

736

737

738

739

740

741

742

743

744

745

746

747

748

Figure legends

Fig 1: CML therapy influence TNT formation in CML cells

(A) TNT quantification of bone marrow samples from 4 different CML patients, results are presented as number of TNTs/100 cells from the average of duplicates. (B) Number of TNTs were quantified in Kcl-22 (memGFP) and K562 (memGFP) cells treated with 100 U/ml of IFNα for 24 h compared to untreated (Ctr) (C) Time-lapse of Kcl-22 cells (memGFP) treated for 1 h with IFNα where images were captured every 10^{th} second for a total of 120 seconds. Arrow heads show movement of memGFP along the TNT structure over time. (D) Kcl-22 and K562 (memGFP) cells were untreated (Ctr) or treated with 5 µM imatinib (Ima) or 100 nM nilotinib (Nilo) for 24 h. (E) Kcl-22 and K562 cells were untreated (Ctr) or treated with 100 nM nilotinib (Nilo) for 1 h. (F) Scanning electron microscopy (SEM) image of a TNT connecting K562 cells treated with 5 µM imatinib (Ima) for 24 h. Jeol JSM-7400F LEI 4.0 kV X3,700 WD 8.0 mm, scale bar =1 µm. (G) Kcl-22 cells treated with 100 nM nilotinib 1 h, fixed with 4 % PFA and stained with phalloidin AF350 followed by anti-β-tubulin staining. Representative images of three independent experiments are shown. Scale bars = 10 µm. (H) Kcl-22 cells were untreated (Ctr) or treated with 100 nM nilotinib (Nilo) for 24 h and TNT quantification was performed before and after addition of CytochalasinD (CytD, 2 µM) for 20 min, at 37°C. (I) Representative fluorescence images from three independent experiments performed in duplicate of Kcl-22 (memGFP) cells with no treatment (Ctr) or treatment with nilotinib (Nilo), cytochalasin D (CytD) or nilotinib (Nilo) followed by cytochalasin D (CytD). Scale bar = 10 µm. For all displayed graphs: Mean ±standard deviation (SD) used together with unpaired t-tests (P**<0.005, P***<0.001, n.s= not significant). All TNT quantifications were performed at least three independent times unless otherwise noted. Fluorescence microscopy was performed by the use of

AxioObserver Z1 fluorescence microscope (Carl Zeiss, Inc, Thornwood, NY) with Alpha Plan Apochromat 63X/1.4 NA Oil DICIII.

Fig 2: BCR-ABL1 effects of TNT formation and cell morphology in Ba/F3 cells

(A) Immunoblotting of Ba/F3 BCR-ABL1 doxycycline (Dox) inducible cells. Ba/F3 cells transduced with empty vector (E.V.) and Ba/F3 transduced with BCR-ABL1 were untreated or treated with 0.1 µM doxycycline for 24 h. Anti-cAbl antibody was used to verify BCR-ABL1 expression. K562 cells were used as positive control and COXIV as loading control. (B) Fluorescence microscopy of Ba/F3 BCR-ABL1 doxycycline inducible cells cultured in the presence or absence of IL-3 and with (+Dox) or without (Ctr) 0.1 g/ml doxycycline, cells were stained with WGA488. Scale bars: = 10 µm. (C) TNT quantification of Ba/F3 transduced with empty vector (black bars) and BCR-ABL1 doxycycline inducible Ba/F3 cells (grey bars) cultured in the presence (+) or absence (-) of IL-3 from 10 % WEHI conditioned medium and with (+) or without 0.1 g/ml doxycycline (-), 1 µg/ml puromycin was present in the culture media in all conditions. (D) Fluorescence microscopy of Kcl-22 and K562 (memGFP) cells untreated (Ctr) or treated for 1 h with nilotinib (Nilo). Scale bar 10 µm. (E) Mass cytometry analysis of down-stream signaling pathways of BCR-ABL1. Results are illustrated by fold changes relative to control (all gated for live cells) based on calculated Arcsinh Ratio of Medians, median from three independent experiments are shown. Microscopy was performed using AxioObserver Z1 fluorescence microscope (Carl Zeiss, Inc, Thornwood, NY) with Alpha Plan Apochromat 63X/1.4 NA Oil DICIII. All data are presented as mean ±standard deviation (SD) and investigated for significance by unpaired t-tests: (P**<0.005). All experiments were performed three times except TNT quantification of Ba/F3 treated with doxocycline and incubated without IL-3 (n=2).

Fig 3: CML cell adherence to fibronectin enhances TNT formation and reduce cell mobility

(A) Kcl-22 (memGFP) cells were pre-treated for 30 min with anti-β1 integrin blocking antibody (10 µg/ml) before seeded in fibronectin-coated IBIDI wells and allowed to adhere for 3 h before treated for 1 h with nilotinib (Nilo) (1 µM) or IFNα (100 U/ml). Cells were investigated by fluorescence microscopy. Scale bars = 10 µm. (B) Cell area of experiments in (A) was measured manually using ImageJ. (C) Cells seeded on fibronectin were tracked for motility by live cell imaging and analyzed using using metamorph and measurements were calculated using Chemotaxis and Migration (IBIDI) plugin in ImageJ. (D) Statistical analysis of motility of the Kcl-22 cells following the different treatment conditions. Significant changes were calculated using unpaired Mann-Whitney test. Mean ±standard deviation (SD) (P*<0.05, P***<0.001, n.s= not significant).

Fig 4: Involvement of Rac1, Rho and Cdc42 GTPases in TNT formation

(A-C) Pull-down assays of active (GTP-bound) Rac1 (A), Rho (B) and Cdc42 (C) were performed with K562 and Kcl-22 cells untreated and nilotinib (Nilo) (100 nM) treated for 1 h. Rac1 and Cdc42 were pulled-down with GST-PAK1-PBD and Rho was pulled-down with GST-Rhotektin-PBD. GTPγS and GDP reactions were performed on Kcl-22 or K562 cell lysates as positive and negative controls, respectively. Proteins were detected by immunoblotting using anti-Rac, anti-Rho (detecting RhoA, RhoB and RhoC) and anti-Cdc42. (D) Kcl-22 and K562 cells were untreated (Ctr) or treated with imatinib (ima) (5 µM) and nilotinib (nilo) (100 nM) for 24 h before immunoblotted with a Tiam-1 antibody. Anti-GAPDH was used as loading control. Quantification of protein bands were performed using the 1D gel analysis tool at Image Quant TL (GE healthcare life sciences version 8.1). (E) TNT quantification of HL-60 and Kcl-22 cells

817 untreated (Ctr) or treated with nilotinib (Nilo) (100 nM) for 24 h. Results are presented as mean
818 ±standard deviation (SD) and significance investigated by the use of unpaired t-tests
819 (P***<0.001, n.s= not significant).

820 **Fig 5: Nilotinib-induced TNT formation in Kcl-22 cells is negatively influenced following**
821 **co-culture with MSCs**

822 (A) SAOS-2 cells were seeded on a fibronectin coated surface one day prior to adding the Kcl-22
823 cells followed by nilotinib (Nilo) (100 nM) treatment or not for 24 h and TNT quantification. As
824 a direct comparison Kcl-22 cells only were untreated or treated with nilotinib (Nilo) (100 nM) for
825 24 h before TNTs were quantified. Results represent three independent experiments performed in
826 duplicates. (B) Kcl-22 cells were incubated in MSC-derived conditioned medium and not treated
827 or treated with nilotinib (Nilo) (100 nM) for 24 h TNTs were quantified and compared to Kcl-22
828 cells incubated in regular medium, untreated (Ctr) and treated with 100 nM nilotinib (Nilo) for 24
829 h. Results represents three independent experiments performed in duplicates. (C-D) Kcl-22 cells
830 were incubated with CXCL8 (20 ng/ml) (C) or VEGF (20 ng/ml) (D) following no treatment or
831 treatment with 100 nM nilotinib (Nilo) for 24 h. TNTs were quantified and compared to Kcl-22
832 cells, untreated or treated with 100 nM nilotinib (Nilo) for 24 h. Results represent three
833 independent experiments performed in duplicates. (E-F) ELISA for CXCL8 (pg/ml) was
834 performed combining supernatants collected from both µ-wells in Fig 5 A and C. Results
835 represent two independent experiments. (G) Flow cytometric analysis of CXCR2 surface
836 expression in Kcl-22 and K562 cells compared to unstained cells. Representative histograms of
837 three independent experiments are shown. (H) Kcl-22 cells were incubated with CXCL8 antibody
838 (0.2 and 0.4 µg/ml) for 24 h followed by TNT quantification. Results represent three independent
839 experiments. (I) Kcl-22 cells treated with different doses of reparixin (1, 10 and 100 nM) for 24h.

Results represent three independent experiments. Y-axis has been changed in figure H and I to better illustrate non-significant changes in TNT numbers. All results are presented as mean ±standard deviation (SD) and unpaired t-test was performed to investigate significance (P**<0.005, P***<0.001, n.s= not significant).

Fig 6: Kcl-22 cell differentiation increase CXCL8 secretion and inhibits the TNT-inducing effect by nilotinib

(A) Kcl-22 cells were treated with ATRA (1 µM) for 5 days in cell tissue flasks before seeded in IBIDI wells and treated with 100 nM nilotinib (Nilo) for 24 h. TNTs were quantified and compared to untreated cells. Results represent three independent experiments preformed in duplicates. (B) ELISA of CXCL8 (pg/ml) on Kcl-22 supernatants from (A). (C) Kcl-22 cells non-treated (Ctr) and treated with ATRA were cytospun and stained with May-Grünwald Giemsa staining. (D) Quantification of differentiated cells was performed by counting at least 100 cells scoring for blast (Bl) and segmented (mature neutrophil granulocyte) (s). Scale bar = 20 µm. Result represent three independent experiments. (E) Flow cytometry analysis of CXCR2 surface expression on Kcl-22 cells without (Ctr) and with ATRA treatment for 5 days. Results represent three independent experiments. Mean ±standard deviation (SD) is demonstrated in the graphs. Results from unpaired t-tests (P*<0.05, P**<0.005).

Fig 7: Illustrated working hypothesis of how TNT formation can be regulated in Kc-22 cells

TNT induction in Kcl-22 was found to be due to increased adhesion to fibronectin coated surfaces through β1-integrin. When CXCL8 was induced by release from stromal cells, adding directly CXCL8 to the cells or inducing release by ATRA treatment, the TNT induced effect by nilotinib was inhibited.

Figure 1

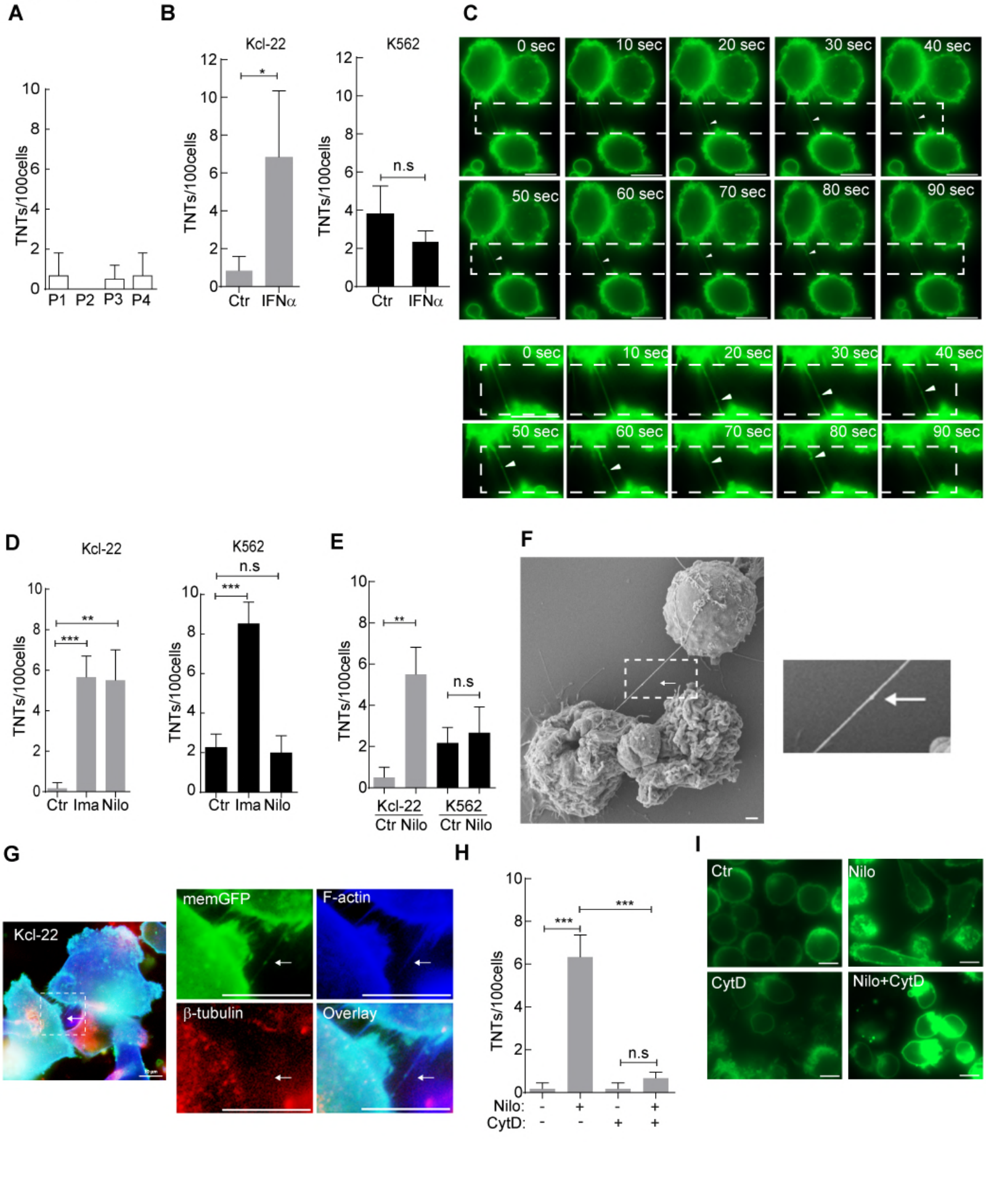

Figure 2

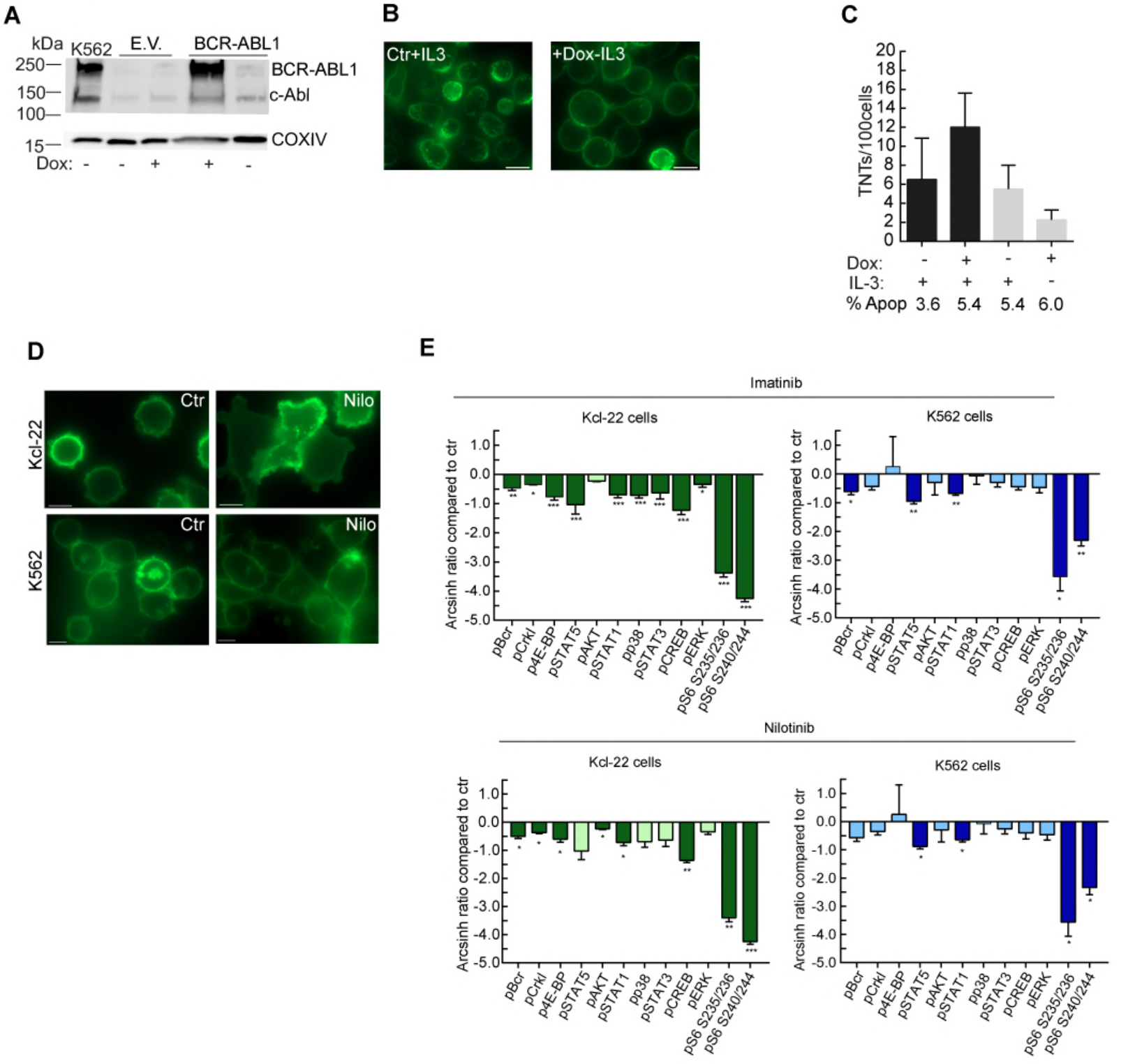

Figure 3

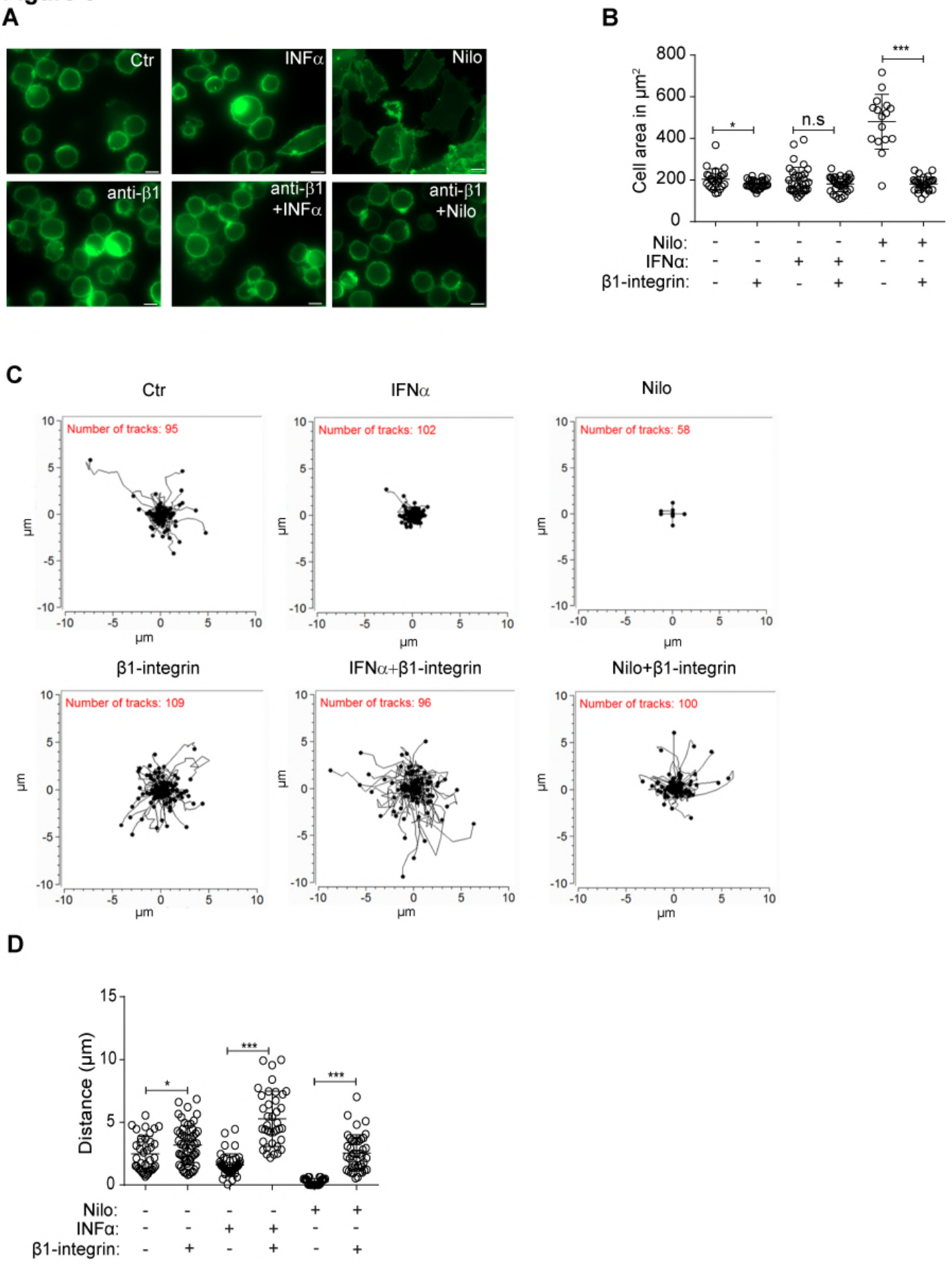

Figure 4

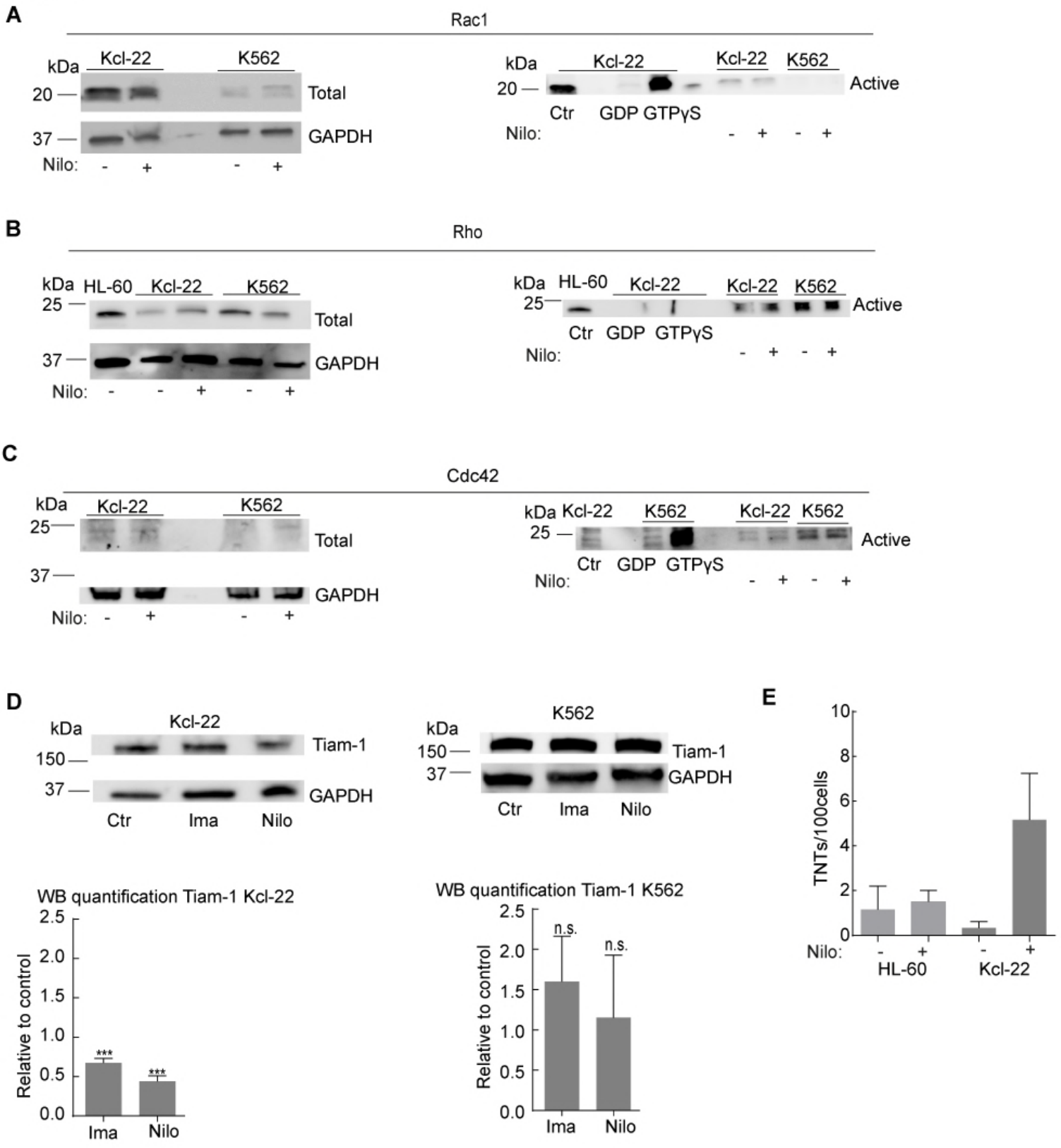

Figure 5

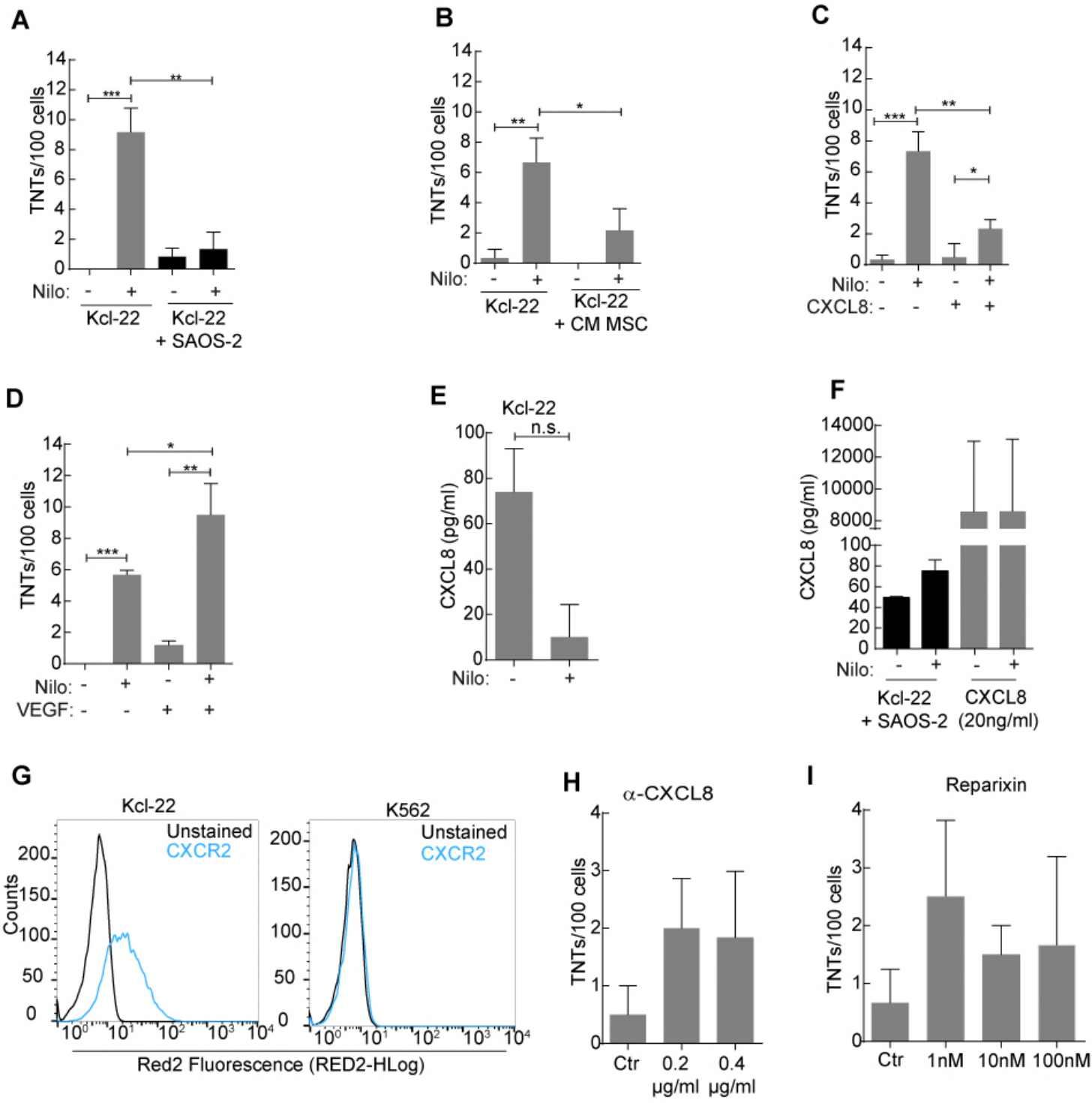

Figure 6

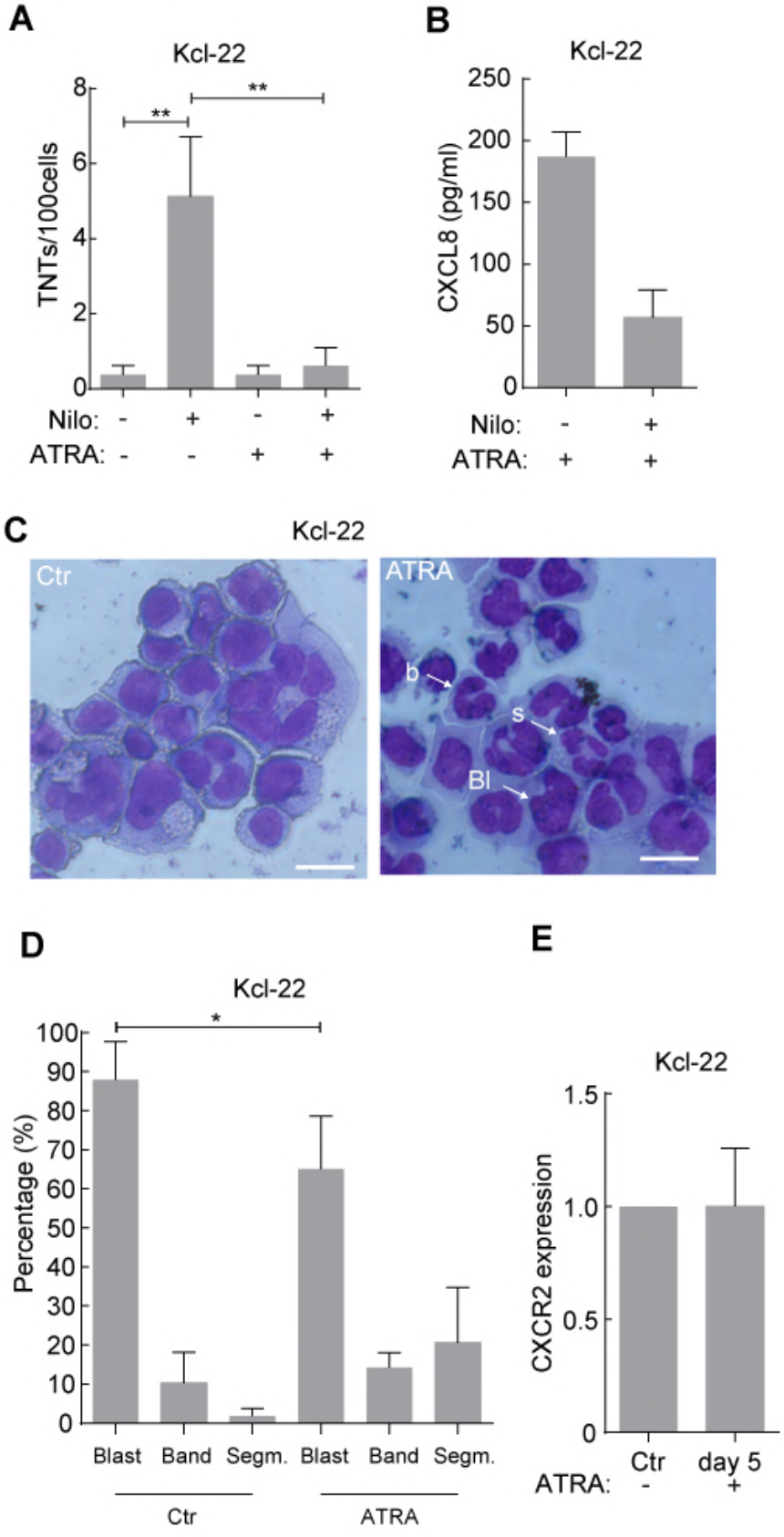

Figure 7

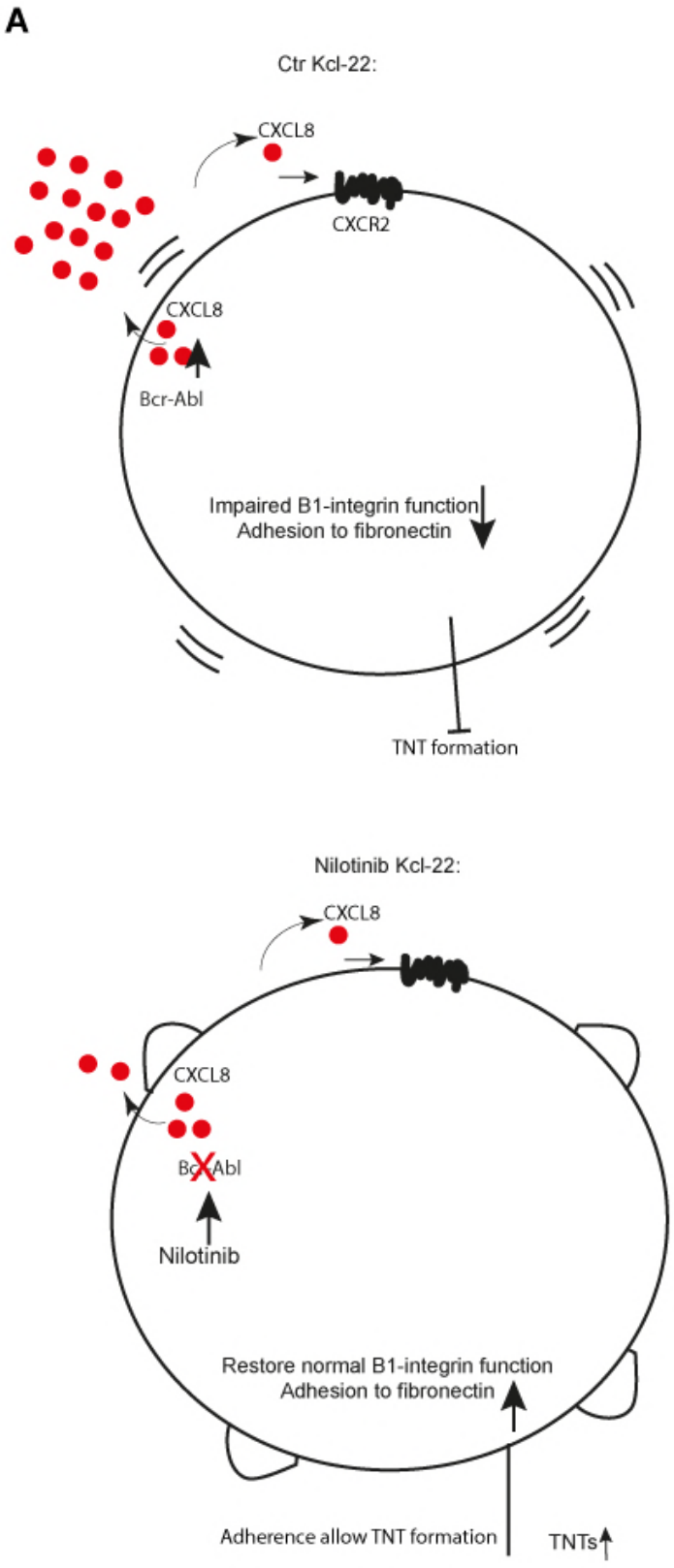

Supplementary figure 1

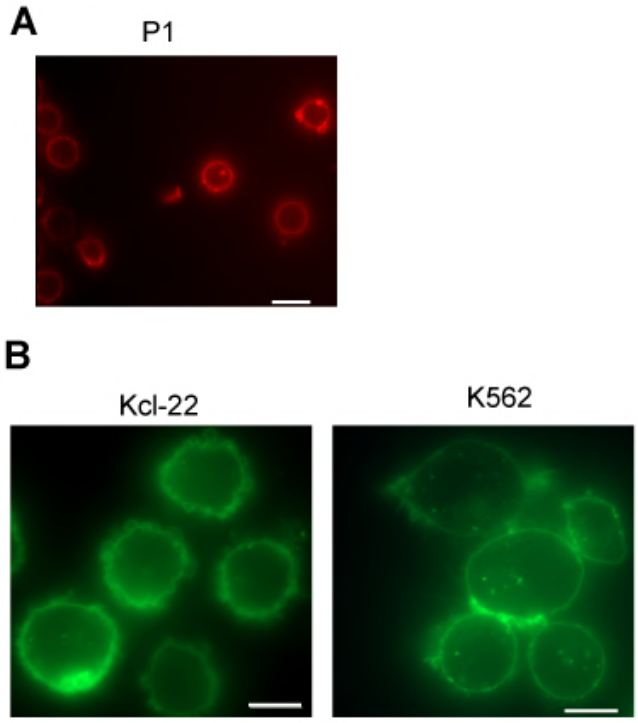

Supplementary figure 2

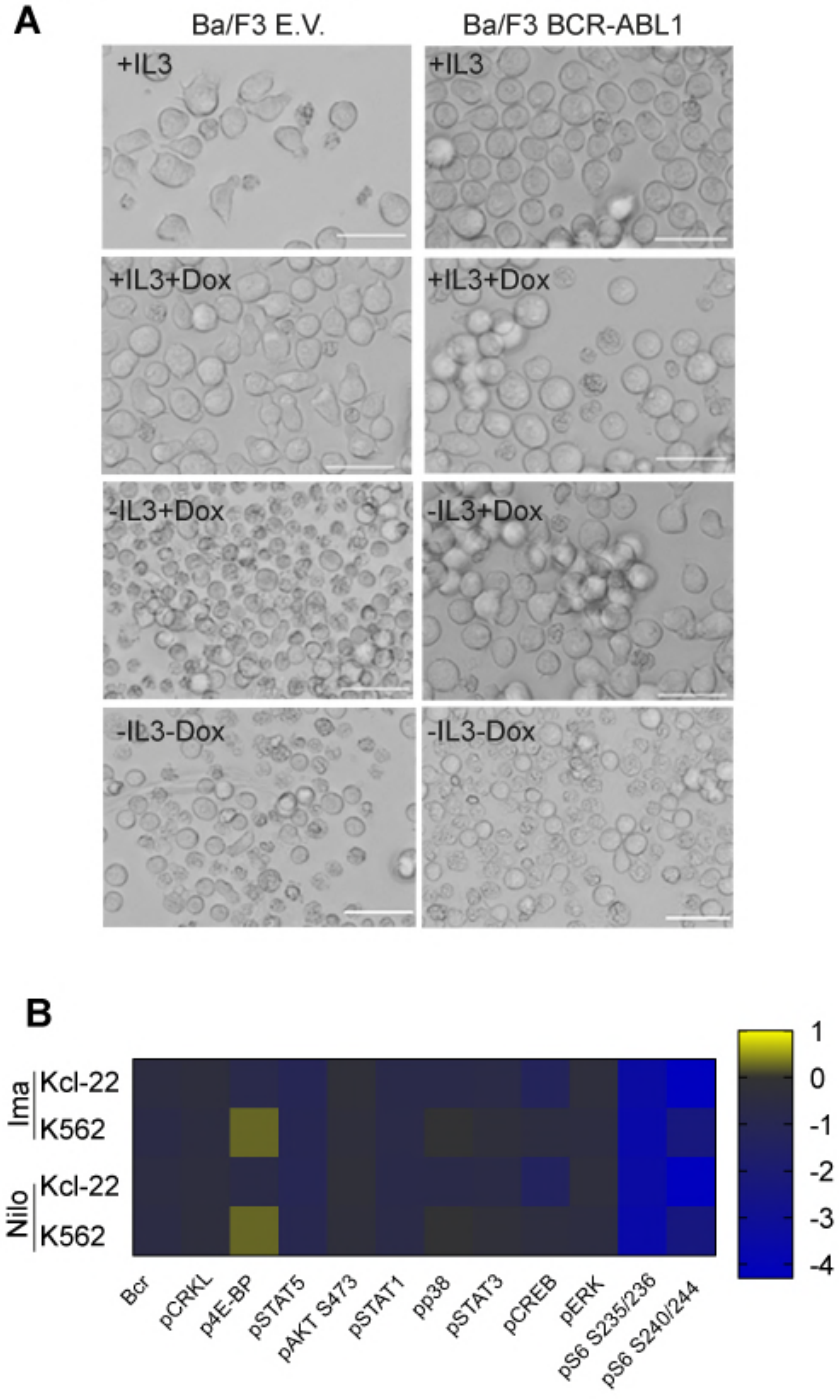

Supplementary figure 3